

Time-Dependent NBI-Heating Simulation of LHD Plasmas Using Toroidal Transport Analysis Linkage Code

Takumi OHNISHI, Kozo YAMAZAKI, Hisamichi FUNABA¹⁾,
Hideki ARIMOTO and Tatsuo SHOJI

Nagoya University, Furo-cho, Chikusa-ku, Nagoya 464-8603, Japan

¹⁾*National Institute for Fusion Science, 322-6 Oroshi-cho, Toki 509-5292, Japan*

(Received 19 November 2007 / Accepted 4 March 2008)

Time-dependent simulation of neutral-beam-heated LHD plasmas has been carried out using the Toroidal Transport Analysis Linkage (TOTAL) simulation code focusing on the time evolutions of beam energy and kinetic energy. This code consists of three-dimensional equilibrium VMEC with bootstrap currents and a one-dimensional transport HTRANS with neoclassical loss determined by ambipolar radial electric field as well as anomalous transport. Neutral beam deposition is calculated using the Monte Carlo code HFREYA, and the slowing down process was calculated using the Fast Ion Fokker-Plank code FIFPC. The simulated time evolution of total energy, including beam energy, roughly agrees with the time evolution of the experimentally measured energy. The temporal change in the beam velocity distribution is also clarified.

© 2008 The Japan Society of Plasma Science and Nuclear Fusion Research

Keywords: NBI-heating, LHD, Fokker-Plank equation, velocity distribution function, neoclassical transport, anomalous transport

DOI: 10.1585/pfr.3.S1081

1. Introduction

In the generation of high-temperature plasmas, neutral beam injection (NBI) heating plays an important role. Since a plasma is heated due to collisions with fast particles injected by an NBI device, the NBI scheme will heat both plasma ions and electrons efficiently in future fusion reactors.

Until now, the simulation of NBI heating in LHD experiments has usually been done in a steady-state manner, and the time-dependent heating process has not been clarified in detail. In this paper, we focused on the time-dependent simulation of neutral-beam-heated LHD plasma, especially, on the time evolution of kinetic energy and beam energy. In the next section, the simulation model is described. The simulation results are shown in Section 3, and the summary is given in the final section.

2. Simulation Model

In order to analyze LHD plasmas heated by the negative-NBI heating scheme, we have used the Fast Ion Fokker-Planck Code (FIFPC) [1], which solves the slowing down process of fast ions, HFREYA code, which computes the deposition of injected neutral particles in helical plasmas, and Toroidal Transport Analysis Linkage (TOTAL) [2, 3] code, which consists of three-dimensional (3-D) equilibrium/1-D transport equations with both neoclassical and anomalous transports.

For the analysis of LHD transport, a 2-D equilibrium-

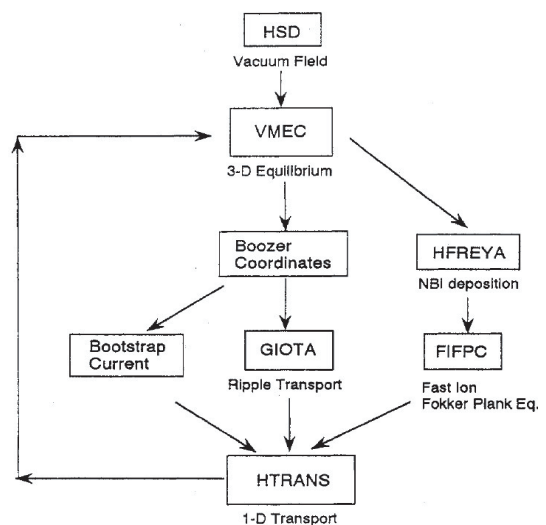


Fig. 1 Schematic flow chart of the TOTAL code.

transport code has been developed in which the 3-D equilibrium code VMEC [4] and the 1-D transport code HTRANS are used. NBI deposition is calculated using the HFREYA code, which is a helical modification of FREYA [5], and the slowing down calculation is done using the Fokker-Planck code FIFPC [1]. The anomalous transport is assumed to fit the global experimental scaling laws, ISS95 scaling law [6], with some confinement improvement factor. The schematic flow chart of this simulation code is shown in Fig. 1.

author's e-mail: t-ohnishi@ees.nagoya-u.ac.jp

2.1 Neoclassical transport

The neoclassical transport losses in helical plasma configurations are divided into an axisymmetric (SYM) tokamak-like part and an asymmetric (ASY) helical ripple part. The effects of the radial electric field $E_\rho (= -e\partial\Phi/\partial\rho)$ are included in the ripple transport simulation [7]. Multiple helicity effects of the magnetic field configuration [8] are taken into account in the $1/\nu$ regime by introducing the form factor ratio of the multi-helicity case to the single-helicity case, F_m/F_s . The multi-helicity form factor F_m is calculated using the GIOTA code [9]. The asymmetric particle and heat fluxes, Γ_{ASYa} and Q_{ASYa} , of species a (electrons ($a = e$) or ions ($a = i$)) as a function of the flux averaged radial variable r are given by

$$\Gamma_{ASYa} = -\epsilon_t^2 \epsilon_h^{1/2} v_{da}^2 n_a \int_0^\infty dx x^{5/2} e^{-x} \frac{\tilde{v}_a(x) A_a(x)}{\omega_a^2(x)}, \quad (1)$$

$$Q_{ASYa} + \frac{5}{2} \Gamma_{ASYa} T_a = -\epsilon_t^2 \epsilon_h^{1/2} v_{da}^2 n_a T_a^2 \times \int_0^\infty dx x^{7/2} e^{-x} \frac{\tilde{v}_a(x) A_a(x)}{\omega_a^2(x)}, \quad (2)$$

where

$$A_a(x) = \frac{1}{n_a} \frac{\partial n_a}{\partial \rho} - \frac{Z_a}{T_a} E_\rho + \left(x - \frac{3}{2}\right) \frac{1}{T_a} \frac{\partial T_a}{\partial \rho}, \quad (3)$$

$$\tilde{v}_a(x) = v_a^0 x^{-1.5} \epsilon_h^{-1} \left\{ \left[\left(1 - \frac{1}{2x}\right) \text{erf}(x^{1/2}) + \frac{1}{(\pi x)^{1/2}} e^{-x} \right] + \bar{z}_a \right\}, \quad (4)$$

$$x = \frac{m_a v_{tha}^2}{2T_a}, \quad (5)$$

$$\omega_a^2(x) = 2.21 \frac{\tilde{v}_a^2}{F_m/F_s} + 1.5(\epsilon_t/\epsilon_h)^{1/2} (\omega_E + \omega_{Ba})^2 + (\epsilon_t/\epsilon_h)^{3/2} \left[\frac{\omega_{Ba}}{4} + 0.6|\omega_{Ba}|\tilde{v}_a(x)(\epsilon_t/\epsilon_h)^{3/2} \right], \quad (6)$$

$$v_a^0 = \frac{4\pi e^4 n_a \ln \lambda}{m_a^2 v_{tha}^3}. \quad (7)$$

Here, ϵ_t is the toroidal inverse aspect ratio (ρ/R), ϵ_h is the helical ripple modulation, n_a is the plasma density, T_a is the plasma temperature, v_{da} is the toroidal drift velocity, v_{tha} is the thermal velocity, ω_E is the $E \times B$ drift, and ω_{Ba} is the ∇B drift frequency. The collision frequency $\tilde{\nu}_a$ is $\nu_e = \nu_{ee} + \nu_{ei}$ with $\bar{z}_e = Z_{\text{eff}}$ for electrons and $\tilde{\nu}_i = \nu_{ii}$ with $\bar{z}_i = 0$ for ions. In the above equations, the ν regime transport was modified. The radial electric field profile is determined by the balance between the asymmetric electron and ion loss fluxes,

$$\Gamma_{ASYe}(E_\rho) = \Gamma_{ASYi}(E_\rho). \quad (8)$$

2.2 Equilibrium analysis

The initial vacuum magnetic surface is calculated using the magnetic tracing code HSD [10] with carefully arranged multi-filament currents. In the present paper, the

free boundary version of VMEC is used. The FCT and bootstrap currents can be included; these currents are estimated to be not large enough to affect the present transport analysis done in this paper. The 3-D magnetic field obtained by the finite beta equilibrium of VMEC is used to evaluate NBI heat deposition and the multi-helicity neoclassical ripple transport coefficients.

2.3 Fokker-Planck equation

To analyze this simulation, we have used FIFPC to solve the Fokker-Planck equation that describes the slowing down process of fast ions. FIFPC may be used alone for treating NBI problems, or in combination with transport codes that describe the evolution of helical core plasmas. The code is designed to calculate the fast ion distribution function in polar coordinates in velocity space at time t . The Fokker-Planck equation, which yields the velocity space fast ion distribution function $f(x, \theta, t)$, is expressed as

$$\begin{aligned} \tau_s \frac{\partial f}{\partial t} = & -\frac{\tau_s}{\tau_{cx}(x)} f + \frac{1}{x^2} \frac{\partial}{\partial x} \left[\left(x^3 - 2Bx + x_c^3 + \frac{C}{x^2} \right) f \right] \\ & + \frac{1}{x^2} \frac{\partial^2}{\partial x^2} \left[\left(Bx^2 + \frac{C}{x} \right) f \right] + \frac{D}{x^3} \left(1 - \frac{D_1}{x^2} + D_2 x \right) \\ & \times \frac{1}{\sin \theta} \frac{\partial}{\partial \theta} \left(\sin \theta \frac{\partial f}{\partial \theta} \right) + E \left(-\cos \theta \frac{\partial f}{\partial x} + \frac{\sin \theta}{x} \frac{\partial f}{\partial \theta} \right) \\ & - \tau_s \frac{\dot{R}(t)}{R(t)} \left[-\left(1 - \frac{1}{2} \sin^2 \theta \right) x \frac{\partial f}{\partial x} + \frac{1}{2} \sin \theta \cos \theta \frac{\partial f}{\partial \theta} \right] \\ & + \tau_s \sum_l \dot{n}_l S_l(x, \theta), \end{aligned} \quad (9)$$

where the terms on the right-hand side are due to charge exchange, drag, speed diffusion, angular scattering, the electric field, compression, and the source of injected fast ions, respectively. The plasma major radius, $R(t)$, is time-dependent due to adiabatic compression; it is not used here. The Spitzer slowing down time τ_s and the charge-exchange lifetime $\tau_{cx}(v)$ are given by

$$\tau_s = 120 \frac{(T_e/1 \text{ keV})^{3/2}}{(n_e/10^{13} \text{ cm}^{-3}) Z_f^2} \frac{m_f}{m_H} \text{ ms}, \quad (10)$$

and

$$\begin{aligned} \tau_{cx}(v) = & \frac{6.6[1 + 1.1 \times 10^{-15} (0.5 m_H v^2)^{3.3}]}{(n_0/10^8 \text{ cm}^{-3})(1 - 0.155 \log 0.5 m_H v^2)^2} \\ & \times \sqrt{\left(\frac{25000 \text{ eV}}{0.5 m_H v^2} \right)} \text{ ms}, \end{aligned} \quad (11)$$

where m_f and m_H are the fast ion mass and the mass of hydrogen, respectively. B , C , D , D_1 , D_2 , and E are constant coefficients given in Ref. [1].

3. Simulation Results

We adopt a typical LHD discharge of shot number 24512 [11] (inward shifted configuration with magnetic axis radius $R_{ax} = 3.6 \text{ m}$; magnetic field strength $B_0 =$

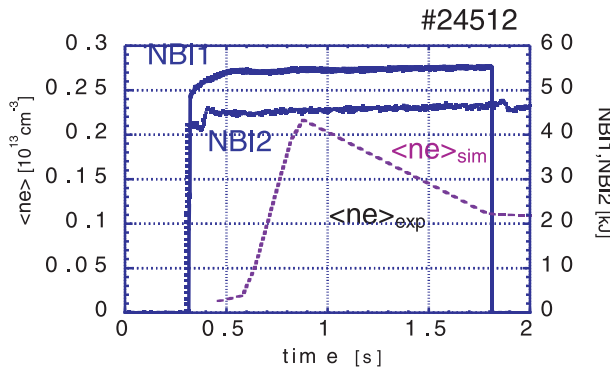


Fig. 2 Experimental value of average electron density $\langle n_e \rangle_{\text{exp}}$ and NBI power NBI 1, 2, and input value of $\langle n_e \rangle_{\text{sim}}$.

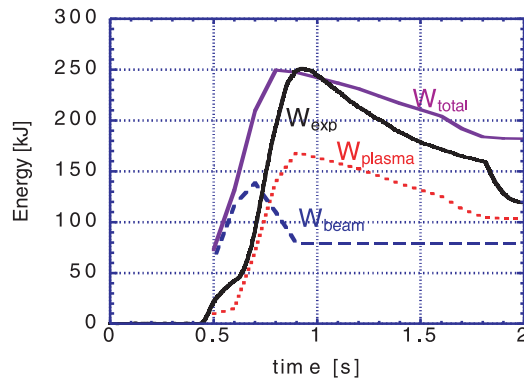


Fig. 3 Time evolution of experimental and simulated beam/plasma energy in LHD.

1.5 T) to investigate the NBI-heating process. The tangential injection beam ion energy, E_b , and beam power, P_b , are 142.9 keV and 4.72 MW, respectively. We have used the input value of average electron density $\langle n_e \rangle_{\text{sim}}$, as shown in Fig. 2. This figure also shows the experimental value $\langle n_e \rangle_{\text{exp}}$ and NBI power.

The simulation results and typical experimental plasma energy data observed by diamagnetic coil measurement are shown in Fig. 3. In the figure, W_{total} is the summation of the simulated kinetic plasma energy, $W_{\text{plasma}} = 3nk(T_e + T_i)/2$, and the beam energy, W_{beam} . In order to compare W_{exp} and W_{total} , we should define $W_{\text{total}} = W_{\text{plasma}} + fW_{\text{beam}}$, where $f \sim 1/5 - 1/3$. The profiles of W_{exp} and W_{total} roughly agree with each other.

Figure 4 shows electron density, n_e , and electron and ion temperatures, T_e and T_i , at 1.4 s. The density profile in the core is flat up to $\rho = 0.6$. The electron temperature in the plasma core is 1.4 keV, and the ion temperature is 0.9 keV.

Figure 5 shows stored beam energy in the plasma at (a) 1.0×10^{-5} s and (b) 0.4 s. The parallel and perpendicular components of stored energy are also plotted in Fig. 5. At 1.0×10^{-5} s, the stored energy are almost completely composed of the parallel component energy. The perpendicular component is very low. At 0.4 s, the perpendicular

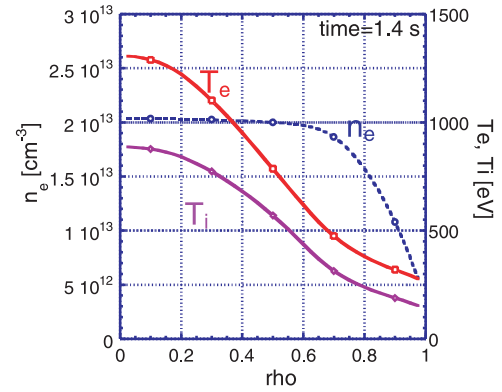


Fig. 4 Profiles of electron and ion temperatures and electron density at 1.4 s obtained in simulation.

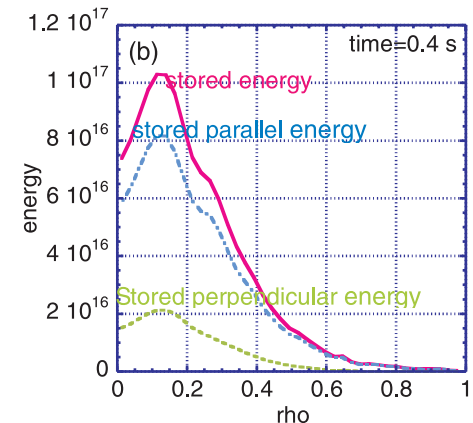
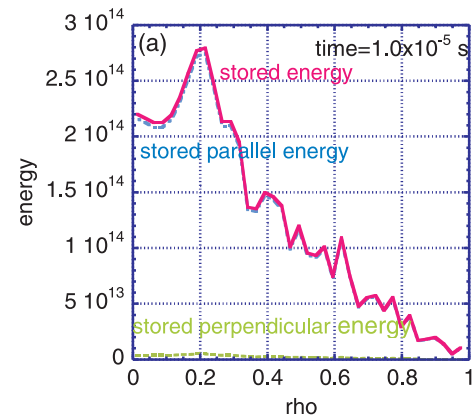


Fig. 5 Profiles of stored energy, parallel energy component, and perpendicular energy component in plasma: (a) 1.0×10^{-5} s, (b) 0.4 s.

component increases to about a quarter of parallel energy. The beam energy is gradually transferred to various angles by diffusion and scattering processes. Therefore, we investigated the distribution function in velocity space in order to analyze the details of energy transfer.

Figure 6 shows the distribution function in velocity space at $\rho = 0.47$. Figures (a), (b), and (c) are profiles of the distribution function at 1.0×10^{-5} s, 0.2 s, and 0.4 s, respectively. At 1.0×10^{-5} s, there are many of high-energy

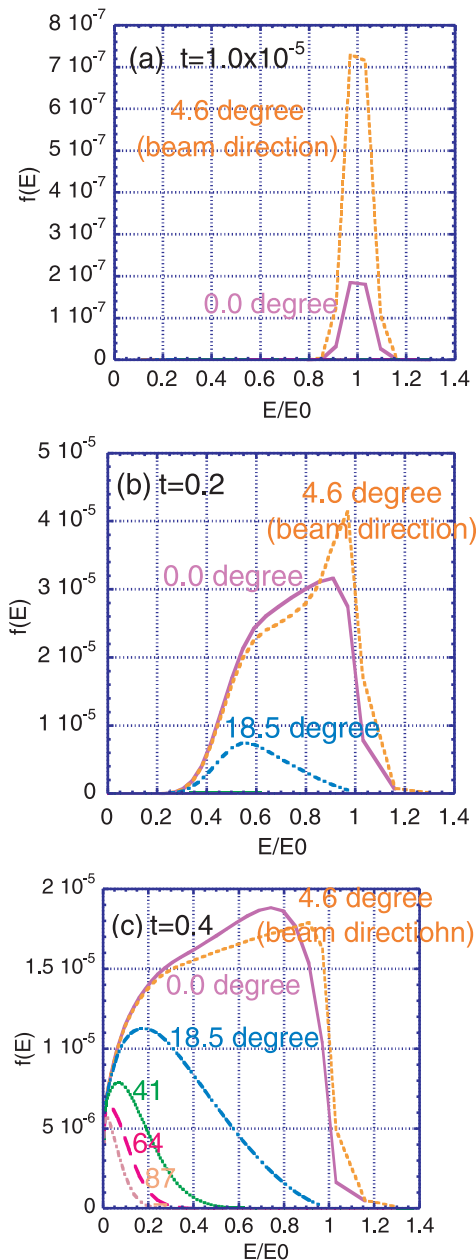


Fig. 6 Distribution function of beam ions calculated by Fast Ion Fokker-Planck Code (FIFPC); (a) 1.0×10^{-5} s, (b) 0.2 s, (c) 0.4 s.

ions at $E/E_0 = 1$. The beam energy is gradually transferred to larger angles.

We can see from Figs. 5 and 6 that the beam only consists of the well-circulating particles, and the most energetic ions are located in the plasma core.

In the code, particle orbit effects can be included by the bounce average orbit in the heating process; however, this effect is not evaluated in the present simulation, because the present discharge analyzed here is a medium-field, low-beta operation. This effect should be included in the low-magnetic field and high-beta plasma case.

4. Summary

We analyzed an NBI-heating time-dependent process using the TOTAL code. The stored energy component is almost parallel just after the injection. Later, the perpendicular energy component gradually increases in the plasma core. We used FIFPC, which solves the velocity distribution of injected fast ions. Directly after injection, there are many ions of high energy at $E/E_0 = 1$. Later, the high-energy ions gradually slow down and transfer energy to the perpendicular component by diffusion and scattering processes.

In summary, the time evolution of simulated total energy, including beam energy, roughly agrees with that of the experimentally measured energy. The temporal change in the beam velocity distribution is also clarified.

- [1] R.H. FOWLER *et al.*, *Comput. Phys. Commun.* **13**, 323 (1978).
- [2] K. Yamazaki and T. Amano, *Nucl. Fusion* **32**, 4 (1992).
- [3] K. Yamazaki *et al.*, *Fusion Eng. Des.* **81**, 2743 (2006).
- [4] S.P. Hirshman, Van RIJ, W.I. Merkel and P. Comput., *Phys. Commun.* **43**, 143 (1986).
- [5] G.G. Lister, D.E., Post and R. Goldston, in *Plasma Heating in Toroidal Devices (Proc. 3rd Symp. Varenna, 1976)*, Editrice Compositori, Bologna 303 (1976).
- [6] U. Stroth, M. Murakami, R.A. Dory, H. Yamada *et al.*, *Fusion* **36**, 1063 (1996).
- [7] D.E. Hastings, W.A. Houlberg and K.C. SHAING, *Nucl. Fusion* **25**, 11 (1988).
- [8] K.C. Shaing and S.A. Horkin, *Phys. Fluids* **26**, 2136 (1983).
- [9] C.L. Hedric, (ORNL), personal communication on the GIOTA code (1988).
- [10] K. Yamazaki *et al.*, *Fusion Technol.* **21**, 147 (1992).
- [11] Ya. I. Kolesnichenko *et al.*, *Phys. Plasmas* **11**, 158 (2004).